ACES Asian Chemical Editorial Society

doi.org/10.1002/asia.202300667

CHEMISTRY AN ASIAN JOURNAL Research Article

www.chemasianj.org

Special Collection

A Platinum(II) Boron-dipyrromethene Complex for Cellular Imaging and Mitochondria-targeted Photodynamic Therapy in Red Light

Aarti Upadhyay,[a] Amrita Nepalia,[b] Arpan Bera,[a] Deepak Kumar Saini,*[b] and Akhil R. Chakravarty*[a]

Cisplatin-derived platinum(II) complexes $[Pt(NH_3)_2(pacac)](NO_3)$ (**1**, **DPP-Pt**) and $[Pt(NH_3)_2(\textbf{Acac-RB})](NO_3)$ (**2**, **Acacplatin-RB**), where Hpacac is 1,3-diphenyl-1,3-propanedione and **HAcac-RB** is a red-light active distyryl-BODIPY-appended acetylacetone ligand, are prepared, characterized and their photodynamic therapy (PDT) activity studied (**RB** abbreviated for red-light BODIPY). Complex **2** displayed an intense absorption band at $\lambda = 652$ nm ($\varepsilon = 7.3\times10^4\ M^{-1}\ cm^{-1}$) and 601 nm ($\varepsilon = 3.1\times10^4\ M^{-1}\ cm^{-1}$) in 1:1 DMSO-DPBS (Dulbecco's Phosphate Buffered Saline). Its emission profile includes a broad maximum at ~673 nm ($\lambda_{ex} = 630$ nm). The fluorescence quantum yield (Φ_F) of **HAcac-RB** and **2** are 0.19 and 0.07, respectively. Dichlorodihydrofluorescein diacetate and 1,3-diphenylisobenzofuran assay of complex **2** indicated photogeneration of singlet oxygen (Φ_Δ: 0.36) as reactive oxygen species (ROS). Light irradiation caused only minor extent of ligand release forming chemo-active cisplatin analogue. The complex showed ~70–100 fold enhancement in cytotoxicity on light exposure in A549 lung cancer cells and MDA-MB-231 multidrug resistant breast cancer cells, giving half maximal inhibitory concentration (IC_{50}) of 0.9–1.8 μM. Confocal imaging showed its mitochondrial localization and complex **2** exhibited anti-metastasis properties. Immunostaining of β-tubulin and Annexin V-FITC/propidium iodide staining displayed complex **2** induced photo-selective microtubule rupture and cellular apoptosis, respectively.

Introduction

The anticancer activity of cisplatin (CP) was first reported by Rosenberg and subsequently of its analogues by others, thereby laying foundation of "platinum-based chemotherapy" for the treatment of various forms of cancers.[1–4] Despite cisplatin's widespread use since approval in 1978, its efficacy remained restricted by limitations such as drug resistance and toxic side effects. The rapid dissociation of two Pt–Cl bonds of CP caused undesired activities that were remedied by the introduction of carboplatin and oxaliplatin, showing reduced side effects due to the presence of slow-releasing O,O-donor ligands. Therefore, regulated production of the aqua form of the platinum(II) drugs precisely within the targeted tumor is one of the best ways to prevent off-target toxicity. In the past decade, there have been reports of the successful release of cytotoxic $\{Pt(NH_3)_2\}^{2+}$ species by application of external stimuli like light as an activator.[5–10] For example, an enhancement in DNA binding of carboplatin was demonstrated as the formation of bifunctional Pt-DNA adducts on UVA light exposure.[5] Similarly, platinum(II) curcumin complexes are known to display the gradual formation of Pt-DNA adducts on visible light irradiation.[6] Therefore, introducing light into cancer therapy provides a new avenue to anticancer drug design to circumvent the problems associated with the conventional drugs belonging to the "platin" family. In that respect, photodynamic therapy (PDT) has emerged as a new combination methodology to treat cancer in the presence of a suitable photosensitizer (PS) appended to a potent chemotherapeutic drug candidate that can be activated by light in the presence of molecular oxygen ($^3O_2$) to generate singlet oxygen ($^1O_2$) as the reactive oxygen species (ROS).[11–16]

PDT involves the activation of an apparently inactive drug precursor to generate singlet oxygen (as ROS) only on light exposure following its administration or localization at the desired cancer/diseased cell target. The *in situ* generated singlet oxygen by a type-II photo-process can lead to cellular apoptosis directly or induce tumor vasculature shutdown. Therefore, utilizing photosensitizer as one of the skeleton elements (ligand) to build multifunctional drug is a promising strategy in chemo-photodynamic synergistic therapy. Further, photosensitizers activable within the "therapeutic window" of 600–800 nm are of relevance in the treatment of cancer as it ensures deeper light penetration in tissues, minimal scattering, and improved tissue compatibility. Thus, combining a near-IR red-light activable photosensitizer appended to an O,O-donor base in our structural design of a platinum(II) complex could display high

[a] A. Upadhyay, A. Bera, Dr. A. R. Chakravarty
Department of Inorganic and Physical Chemistry
Indian Institute of Science
Bengaluru 560012, Karnataka (India)
E-mail: arc@iisc.ac.in

[b] A. Nepalia, Dr. D. K. Saini
Department of Developmental Biology and Genetics
Indian Institute of Science
Bengaluru 560012, Karnataka (India)
E-mail: deepaksaini@iisc.ac.in

Supporting information for this article is available on the WWW under https://doi.org/10.1002/asia.202300667

Special Collection This manuscript is part of an Indo-German Workshop (IGW) special collection.

PDT activity from the metal-bound PS with high singlet oxygen quantum yield. In case of any undesirable release of the PS generating a chemo-active cisplatin analogue, the process could offer a co-treatment strategy owing to diverse modes of action of PDT of the released ligand and chemotherapy from the CP analogue.

Among different types of fluorescent dyes and photosensitizers, tetrapyrrolic porphyrin dyes were extensively used in PDT. Photofrin®, as the FDA approved PDT drug, causes skin sensitivity and hepato-toxicity leading to jaundice.[17] Such tetrapyrrolic dyes in general show reduced activity on binding to a metal. In that respect, the dipyrrolic BODIPY (boron-dipyrromethene) dyes have emerged as alternatives in biological molecule detection, tumor imaging, and photothermal and photodynamic therapies.[18–20] Their remarkable photophysical properties showing intense absorption at relatively long wavelength, high stability, facile high yield synthesis with tunable core, and desirable optoelectronic properties have enabled their use as photosensitizers in PDT.[21–25] To this effect, we have reported BODIPY conjugates of platinum(II) complexes of curcumin demonstrating generation of singlet oxygen in moderate yield on red light photoirradiation showing IC_{50} values within 1.3-6.9 μM in A549 (lung epithelial cancer cells) and MDA-MB231 (breast cancer cells) cancer cells while remaining inactive in dark.[26]

To develop new types of photoactive platins showing red-light PDT activity, our group has recently reported **Maloplatin-B**, having a methyl malonyl chloride derivative of BODIPY as a bidentate O,O-donor ligand.[27] This complex behaved as a potential "chemo-PDT" agent showing photocytotoxicity in the range of 1.6-2.4 μM in A549 and HeLa cells. With an objective to improve this model, we have now designed a new platin, namely, $[Pt(NH_3)_2$(**Acac-RB**)$](NO_3)$ (**Acacplatin-RB**, **2**), in which acetylacetone is covalently conjugated to a distyryl-BODIPY unit as a bidentate O,O-donor ligand as PS that is bound to $\{Pt(NH_3)_2\}^{2+}$ moiety of cisplatin. The basic skeletal of acetylacetone ligand strongly resemble those of the O,O-donor ligands in oxaliplatin and carboplatin.[4b] Complex **2** absorbs strongly in the photo-therapeutic window, making it suitable for PDT activity, and is observed to be remarkably photostable with minor photo-release of cisplatin species, which could possibly form cyto-lethal Pt-DNA crosslinks to a lesser extent. Herein, we report two new platinum(II) complexes, namely, $[Pt(NH_3)_2$(pacac)$](NO_3)$ (**1**, **DPP-Pt**) as a control species and $[Pt(NH_3)_2$(**Acac-RB**)$](NO_3)$ (**2**, **Acacplatin-RB**) as PDT active complex, where Hpacac is 1,3-diphenyl-1,3-propanedione, and **HAcac-RB** is a red-light active distyryl-BODIPY appended acetylacetone ligand (**RB** is abbreviated for red-light BODIPY) (Figure 1). Along with remarkable anticancer activity and strong red luminescence, complex **2** was found to be useful for cellular imaging and other mechanistic studies. The significant results of this work include a high molar absorptivity value of **2**, red light photocytotoxicity in sub-micromolar concentrations, photostability of the complex, high yield singlet oxygen generation, prominent mitochondrial localization and apoptotic cell death. These findings highlight the positive impact of platinum(II) coordination to the BODIPY dye resulting significant photodynamic therapy activity in red light when the ligand itself showed significantly lower activity.

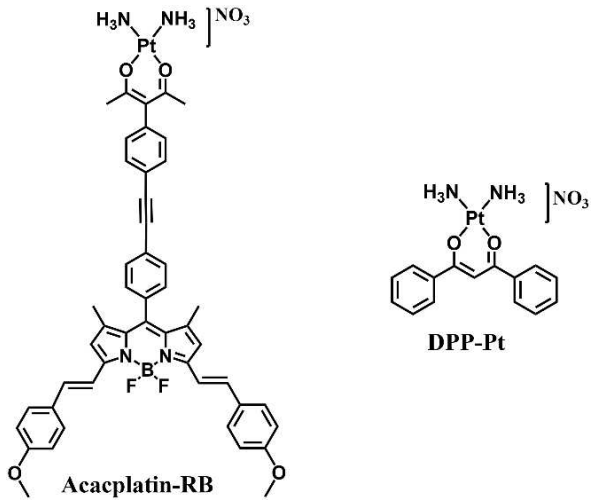

Figure 1. Chemical structures of the platinum(II) complexes $[Pt(NH_3)_2$(pacac)$](NO_3)$ (**DPP-Pt, 1**) and $[Pt(NH_3)_2$(**Acac-RB**)$](NO_3)]$ (**Acacplatin-RB, 2**).

Results and Discussion

Synthesis and General Aspects

The synthetic steps for acetylacetone (Hacac) derivative having covalently linked red-light activatable boron-dipyrromethene (**HAcac-RB)** and complexes **DPP-Pt** (**1**) and **Acacplatin-RB** (**2**) are designed and prepared as shown in Schemes S1, S2 (vide SI).[28] **HAcac-RB** was synthesized by Sonogashira coupling of acetylacetone linked to phenyliodo derivative "**B"** with terminal alkyne appended BODIPY conjugate "**F"** as shown in the schemes. Complex **2** was prepared from a reaction of cisplatin with $AgNO_3$ with successive addition of deprotonated **HAcac-RB** in DMF medium. The compounds were characterized using NMR and mass spectral data (Figures S1-S9). The purity of the metal compounds was assessed from the elemental analysis data. Selected physicochemical data are presented in Table 1. **HAcac-RB** ligand and its platinum(II) complex **2** displayed a singlet peak at 6.65 ppm and 6.98 ppm, respectively, in ^{1}H NMR spectra. The peak is assignable to the pyrrole –CH proton of the BODIPY core. Both compounds showed characteristic peaks of disubstituted styryl BODIPY. The downfield shift of the aromatic peaks from 7.22–7.72 ppm of the ligand to 7.39–7.96 ppm in its Pt(II) complex supported the coordination of the acac-BODIPY ligand to the metal. The fingerprint peaks of NH_3 protons of **2** were observed at 4.58 ppm. A single signal in the ESI-MS spectra with m/z value of 452.0997 (for **DPP–Pt**, **1**) and 986.3242 (for **2**) was assignable to $[M\text{-}NO_3]^+$, indicating formation of the metal complexes. Characteristic isotopic distribution patterns supported the presence of platinum (Figures S8, S9). The molar conductance values in the range of

Table 1. Physicochemical data of the ligand and the complexes.

Compound→	HAcac-RB	DPP-Pt (1)	Acacplatin-RB
Λ_M[a]/S m^2 mol^{-1}	–	68	74
UV – visible[b]: λ_{max}/ nm (10^{-4} ε/M^{-1}cm^{-1})	651 (8.8), 601 (3.1, sh), 377 (5.6)	331 (3.1), 383 (1.6)	652 (7.3), 601 (3.1), 377 (5.4)
Emission[c] λ_{em} /nm (Φ_F)	670 (0.19)	–	673 (0.07)
$^1O_2$ quantum yield (Φ_Δ)[d]	0.18	–	0.36
^{1}H NMR δ/ppm of β-protons[e]	6.65	–	6.98

[a] Molar conductivity was recorded in DMF. [b] In 1:1 (v/v) DMSO/DPBS medium; sh, shoulder. [c] Wavelength of emission maxima in 1:1 (v/v) DMSO/DPBS and fluorescence quantum yield (Φ_F) in DMSO. [d] Singlet oxygen quantum yield in DMSO. [e] ^{1}H NMR recorded in $CDCl_3$ for the BODIPY ligand and DMSO-d_6 for complex **2** (**Acacplatin-RB**).

68–74 S m^2 mol^{-1} in DMF suggested 1:1 electrolytic behaviour of the complexes **1** and **2**.

The absorption spectra and emission properties of the ligand and complexes **1** and **2** were studied in 1:1 (v/v) DMSO/DPBS solution. Complex **2** displayed BODIPY based absorption profiles with an intense maximum at λ = 652 nm (ε = 7.3×10^4 M^{-1} cm^{-1}) with a shoulder peak at λ = 601 nm (ε = 3.1×10^4 M^{-1} cm^{-1}) (Figure 2). The strong absorption bands in the region of lower energy were resulted from the conjugation of the methoxy containing distyryl units to the BODIPY core. It is noteworthy that the strong absorption band within the photo-therapeutic spectral window offers an opportunity for deep tissue penetration and thus, complex **2** potentially suitable for PDT evaluation. As expected, the absorption pattern of the ligand resembled strongly to that of its complex **2** with λ_{max} = 651 nm and ε = 8.8×10^4 M^{-1} cm^{-1}. The control complex **DPP-Pt** (**1**) displayed an absorption band at 331 nm (ε = 3.1×10^4 M^{-1} cm^{-1}) and 383 nm (ε = 1.6×10^4 M^{-1} cm^{-1}). Lack of any absorption bands in the visible region for **1** in the absence of a BODIPY moiety made it PDT inactive. Complex **1** was used as a control species. Both **HAcac-RB** and **2** displayed strong emission spectra with respective maxima at 670 nm and 673 nm on 630 nm (λ_{ex}) excitation in 1:1 (v/v) DMSO/DPBS solution. The fluorescence quantum yield of the compounds was obtained using the integrating sphere method in DMSO. The Φ_F value for the BODIPY ligand and its platinum(II) complex was 0.19 and 0.07, respectively (Figures S10, S11). The fluorescence characteristics of complex **2** were utilized to study its intracellular localization and its mode of cellular internalization. The lower Φ_F value for **2** than the BODIPY ligand is due to the heavy atom effect of platinum metal facilitating the singlet to triplet intersystem crossing (ISC). This has resulted in a significantly high singlet oxygen quantum yield (Φ_Δ) value of **2** than the ligand (Table 1).

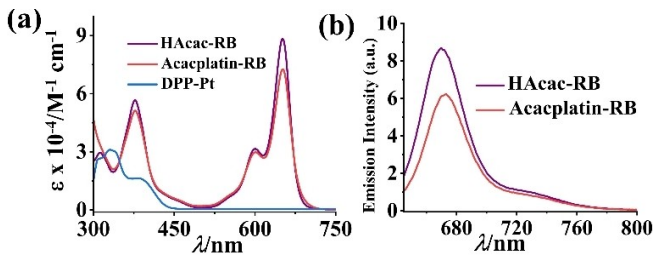

Figure 2. (a) The electronic absorption spectral profiles of ligand **HAcac-RB**, and the complexes **DPP-Pt** (**1**) and **Acacplatin-RB** (**2**). (b) Emission spectra of **HAcac-RB** and **Acacplatin-RB**, both excited at λ = 630 nm. The spectra were recorded in 1:1 (v/v) DMSO:DPBS (Dulbecco's phosphate-buffered saline) at pH 7.2.

Solubility and stability

Good solubility of the ligand **HAcac-RB** was observed in dimethyl sulfoxide (DMSO), dimethylformamide (DMF), dichloromethane, and ethyl acetate. Its solubility was moderate in methanol and acetonitrile, and it was essentially insoluble in diethyl ether and hexane. Complex **Acacplatin-RB** (**2**) showed good solubility in DMSO, DMF, and chlorinated solvents. It was moderately soluble in acetonitrile and methanol, and sparingly soluble in ether and hydrocarbons. The solubility of the control complex, **DPP-Pt** (**1**) resembled that of **Acacplatin-RB** (**2**). They showed good solubility in methanol and acetonitrile. The photostability of the BODIPY ligand and its complex was studied. Such a study is of importance as any decomposition of a photosensitive drug usually causes poor therapeutic efficacy or undesired side effects and brings strong interference to diagnosis and treatment. Time-dependent UV-visible spectra of **HAcac-RB** and **Acacplatin-RB** were recorded in 1:1 (v/v) DMSO/DPBS solution under the same conditions for 72 h (Figure S12). No apparent changes in the spectral features were observed for both indicating their excellent stability. Drug stability in various physiological pH, in general, helps in designing the formulation. Human gastrointestinal fluid pH covers a wide range from 1 to 8. Therefore, the integrity of the complex at alkaline (pH = 8) and acidic (pH = 3) solutions was examined using UV-visible spectroscopy (Figure S13). Two solutions of complex **2** in 10% DMSO-DPBS at pH = 3 and pH = 8 were kept in the dark for different time intervals, and their spectral features were recorded for 48 h. Only negligible bleaching was observed from the absorption spectral intensity at each pH for this period. The intact behaviour in the highly acidic condition is of significance

for possible oral administration of complex **2** in any future clinical trials.

Theoretical Studies

Theoretical calculations were performed using DFT (Density Functional Theory) for structural insights, electronic properties, and frontier orbital's distribution of **Acacplatin-RB** (**2**) and **DPP-Pt (1)** (Figure 3, Figure S14).[29a] The calculations were performed using B3LYP (Becke, 3-parameter, Lee-Yang-Parr) functional with basis sets LanL2DZ for Pt and 6–311G for C,H,N,B,F,O. Computations were performed in Gaussian09 suites.[29b] The energy optimized structure showed a typical square planar geometry around the metal center. The ammine ligands are at 2.098 Å (Pt–N distance) from the platinum, while the acetylacetone derivative chelates the metal centre at a mean distance of 2.003 Å (Pt–O). The coordinates of optimized structures are listed in Tables S1, S2 (vide SI). For the electronic structure, the HOMO wave functions were observed to be well delocalized over the BODIPY skeleton along with distyryl extension (Figure 3). The localisation of LUMO is towards platinum bound acetylacetone unit. In **DPP-Pt** where BODIPY is absent, HOMO and LUMO localised over 1,3-diphenyl-1,3-propanedionate ligand. This energy minimization of the active complex, **Acacplatin-RB** was further followed by TD-DFT calculations to theoretically predict electronic transitions along with the orbital contributions. Significant transitions are listed in Table S3 (vide SI). Theoretical λ_{max} for **Acacplatin-RB** was found to be 601 nm with a good oscillator strength value of 0.92 and the corresponding transition is assignable from HOMO to LUMO + 3. The predicted value is in moderate agreement with the experimental value of λ_{max} of 652 nm (Table 1).

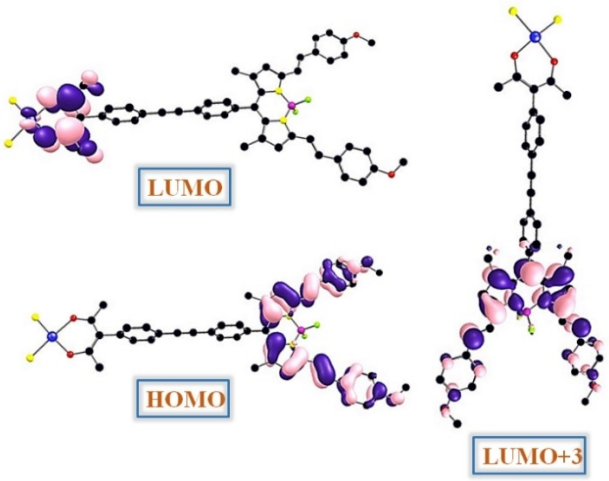

Figure 3. Computational studies using B3LYP/LANL2DZ (for Pt) and 6–311G (for O, N, B, F, C, and H) functionals performed on **Acacplatin-RB** (**2**) to obtain the electronic distributions of molecular orbitals involved in transitions in the near-IR region. Hydrogen atoms are omitted for clarity.

Photo-release of ligand and 9-ethylguanine binding

The photo-release of the O,O-donor acac-based ligands from their platinum(II) complexes is well documented in the literature.[6,7,10] Release of a photosensitizer ligand on near-IR light exposure could provide a platform for synergistic chemotherapy and photodynamic therapy within the biological window. Such a release is, however, expected to reduce the PDT activity of the complex significantly, considering the higher singlet oxygen quantum yield of the complex **2** than its BODIPY ligand **HAcac-RB** (Table 1). Any possible photo-responsive changes in the emission intensity of **Acacplatin-RB** (10 μM) were monitored on light irradiation (red light diode laser, $\lambda =$ 642 nm) and in the dark. Interestingly, only a minor enhancement in fluorescence intensity was noted on photo-irradiation when compared to that of the unexposed sample (Figure S15). Since, the emission of BODIPY ligand is reduced on metal complexation, an increase of emission intensity on photo-exposure indicates some release of the free ligand. Also, red light-triggered changes were studied using mass spectrometry. Mass spectrum of the irradiated sample displayed only a minor presence of the free ligand, whereas no peak of the free ligand was observed in the light unexposed sample spectrum (Figure S16). In addition, no noticeable changes in the spectra were observed in the time-dependent NMR study. The released species with a cisplatin analogue could show some chemotherapeutic effect but with reduced PDT effect, as the free BODIPY ligand has a significantly lower Φ_Δ value than complex **2**. The overall effect of the two released species is expected to be considerably lower than the PDT effect of **Acacplatin-RB** (**2**).

The basic chemotherapeutic mechanism is believed to be the DNA-binding behaviour of bioactive Pt(II) species. Therefore to discover any post-release behaviour of active $\{Pt(NH_3)_2\}^{2+}$ species, photo-irradiation was performed in the presence of pyridine as a trapping agent. A 20 μM solution of **Acacplatin-RB** (20 μM in 10% DMSO-PBS) and pyridine (10 μl) was exposed to red light ($\lambda = 642$ nm) and was subjected to mass spectral analysis. A significant peak of 193.5487 m/z with platinum's isotopic distribution pattern assignable to $[Pt(NH_3)_2(py)_2]^{2+}$ appeared along with a 759.3349 m/z peak of the free BODIPY ligand, **HAcac-RB** in the case of the light-exposed solution (Figure S17). Both peaks were absent in the solution kept in the dark. The photo-released Pt(II) derivative with a $\{Pt(NH_3)_2\}^{2+}$ moiety is likely to form an aquo species capable of binding to ds-DNA. The photo-triggered binding ability of **Acacplatin-RB** was studied by using a model nucleobase, namely, 6-amino-9-ethyl-2-hydroxypurine (9-ethylguanine, EtG) and was analysed using mass spectrometry. Photo-irradiation of a mixture of **Acacplatin-RB** and EtG in 1:1 DMSO/H_2O showed formation of Pt(II)-EtG bis-adduct, $\{Pt(EtG)_2\}^{2+}$ (m/z 276) and Pt(II)/EtG monoadduct along with the solvent molecule, DMSO in $[Pt(NH_3)(EtG)(DMSO)]^{2+}$ giving m/z of 234 (Figure S18). Binding studies of **Acacplatin-RB** with EtG thus provided strong evidence that the photo-released cisplatin can bind to nucleophilic DNA effectively.

The DNA crosslink formation was also ascertained by observing changes in binding of ethidium bromide (EB) in ct-

DNA in the presence of **Acacplatin-RB** by emission spectroscopy. Ethidium bromide (EB) is a flat aromatic dye that readily inserts itself between the base pairs of DNA. It doesn't exhibit a strong preference for any specific base pairs and has a moderate binding affinity, which varies with ionic strength ($K_{EB} = 10^4$ - 10^6 M^{-1}). [30a] When EB intercalates, it causes a 26° unwinding of the DNA base pairs near the insertion site, offering insights into the flexibility of DNA's conformation.[30b] EB being a highly useful tool in fluorescence spectroscopy for examining DNA conformation is employed in competitive binding studies to investigate how other substances bind to DNA. [30c] A decrease in the emission intensity of EB (50 μM) at λ = 595 nm, when this solution was treated with **Acacplatin-RB** (20 μM) and subjected to red light (λ = 642 nm, 30 min) exposure suggested Pt-DNA adduct formation while the emission spectra of EB remained unaltered in dark (Figure S19). The overall data provided evidence for photo-activated ligand release only to a minor extent, thus making **Acacplatin-RB**, a potential red light-activated anticancer agent.

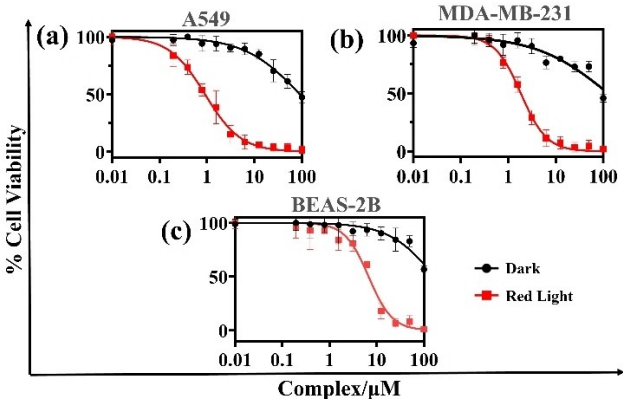

Figure 4. Cell viability plots showing % viability as obtained in **Acacplatin-RB** (**2**) treated in (a) A549, (b) MDA-MB-231, and (c) BEAS-2B cells for 4 h in dark and then subjected to either photo-irradiation (λ = 600-720 nm, light dose = 30 Joules cm^{-2}, red squares) or left in dark conditions (dark, black circles). The complex containing media after light exposure was replaced with fresh media and was incubated for an additional 20 h. The experiment was performed in triplicates.

Photocytotoxicity in red Light

To analyse the therapeutic potential of the compounds, photocytotoxicity was assessed in model lung cancer cells, A549 and human epithelial breast adenocarcinoma cells, MDA-MB-231 and human non-tumorigenic lung epithelial BEAS-2B cells. MTT (3-(4,5-dimethylthiazol-2-yl) − 2,5-diphenyltetrazolium bromide) dye was used for assessment of cell viability. The assay was performed in two sets, one set was photo-irradiated using red light (λ = 600-720 nm; light dose = 30 Joules cm^{-2}) after 4 h incubation, while the other set was kept in dark unexposed to light. The observed IC_{50} values are listed in Table 2.[31] **Acacplatin-RB** on red-light activation showed excellent phototoxicity (IC_{50} = 0.9 μM in A549 cell lines) with 100-fold enhancement compared to unexposed A549 cells (IC_{50} = 90.5 μM) (Figure 4, Figure S20). This increase is due to significant generation of reactive oxygen species from the platinum(II) bound BODIPY ligand. Interestingly, the IC_{50} value of **Acacplatin-RB** (**2**) is nearly half as compared to that of Maloplatin-B (IC_{50} = 1.6 μM).[27] It is also more cytoactive than other Pt(II)-BODIPY complexes, such as Pt-BDPA complex reported by He and co-workers (Table S4, BDPA = BODIPY derivative of dipicolylamine).[31(a)] In contrast, ligand **HAcac-RB** exhibited significantly lower photoactivity (IC_{50} = 54.12 μM in A549 cells) as compared to its platinum(II) complex because of remarkable enhancement in singlet oxygen production involving the BODIPY unit. The ligand was non-toxic in the dark, giving IC_{50} > 100 μM. The photo-inactivity of **DPP-Pt** (IC_{50} > 100 μM) in A549 cells highlights the importance of the BODIPY unit for red light PDT activity. The cytotoxic activity of **2** was also studied in multidrug resistant cancer cell line, MDA-MB-231. Interestingly, it showed efficient photoactivity giving IC_{50} of 1.8 μM while being inactive in dark. Thus, complex **2** exemplifies a high-efficacy photocytotoxic agent suitable for photo-therapeutic applications. Interestingly, both complex **2** and the ligand displayed lower photocytotoxicity with IC_{50} value of 6.7 μM and 84.0 μM in non-tumorigenic BEAS-2B cell line, possibly due to better uptake of **2** in the cancer cells than in the normal cells.

Cellular Uptake

The cellular uptake of the ligand, **HAcac-RB**, and its complex, **Acacplatin-RB** (**2**) was studied using the Flow Cytometry approach. A549 cells were treated with the ligand (1 μM) and the complex (1 μM), separately, and were incubated for 2, 4, 5,

Table 2. Photocytotoxicity data[a] giving IC_{50} values of the ligand and the complexes along with cisplatin.

Cells/Complex	A549 Light[b] [dark[c]]	MDA-MB-231 Light[b] [dark[c]]	BEAS-2B Light[b] [dark[c]]
HAcac-RB	54.1 ± 2.6 [> 100]	70.5 ± 3.2 [> 100]	84.0 ± 1.6 [> 100]
Acacplatin-RB (**2**)	0.9 ± 0.1 [90.5 ± 3.4]	1.8 ± 0.3 [> 100]	6.7 [> 100]
Cisplatin[d]	32.5 ± 2.5 [35.0 ± 2.2]	–	–

[a] IC_{50} values are in μM. Complex **DPP–Pt** in dark and light gave IC_{50} values > 100 μM in all the three cell lines. [b] Cells were treated with the compounds and were incubated for 4 h followed by exposure to red light of 600–720 nm (L, Light Dose: 30 Joules cm^{-2}) with subsequent post incubation of 19 h in dark. [c] In dark, similar conditions as that of light experiment but without any exposure to red light. Cells were incubated in dark throughout 24 h of time-period. [d] IC_{50} of cisplatin is taken from ref [31(b)].

and 6 h. After thorough washings of DPBS (Dulbecco's phosphate-buffered saline), the fluorescence of the internalized complex was detected using APC–Cy7 (λ_{exc} = 640 nm) channel in FACS (fluorescence-activated cell sorting) Verse instrument. Observation of a significant increment in the fluorescence indicated significant uptake of both the ligand and the complex. Corresponding histogram (representing fluorescence intensity) of the cells treated for 2 and 4 h showed significant displacement in a successive manner from unstained controls indicating the active uptake of the ligand (Figure 5(a)). A majority of the complex got internalised within 2 h as there was only a marginal increase from 2 to 4 h (Figure 5(b)). Considering no apparent shift after 4 h i.e., on 5 and 6 h, the uptake of the ligand and the complex took place almost entirely within 4 h of incubation. Along with the rapid internalization, the cellular uptake of complex **2** was higher than that of **HAcac-RB**. In addition, the red luminescent trait of the complex was employed to determine the mechanistic pathway of cellular internalization using confocal microscopy (Figure 5(c)). Complex **2** added A549 cells were incubated at 4 °C and 37 °C for 4 h to assess whether the mode of uptake was reliant on energy or not. A549 cells, incubated at higher temperature, appeared bright red in confocal imaging whereas nominal red emission was observed in that of lower temperature set. The results suggest probably endocytosis of complex **2** in A549 cells (Figure 5(c)).

ROS generation

Incorporation of heavy metals like platinum in the fluorogenic scaffold of BODIPY based ligands is known to enhance ROS (reactive oxygen species) generation due to populated excited triplet states.[32] In complex **2**, the ligand **HAcac-RB** in mono-anionic form is bound to platinum for increased production of oxidative stress on photo-irradiation in the PDT spectral window. The *in-vitro* ROS production was analysed by DCFDA (2,7-dichlorofluorescein diacetate) assay by confocal laser scanning microscopy (CLSM) (Figure 6(a)). DCFDA is a cell-permeable dye, which after internalization, undergoes deacetylation followed by oxidation in the presence of cellular ROS to generate a green fluorescing compound, DCF (2′,7′-dichlorodihydrofluorescein) of λ_{em} = 525 nm (λ_{ex} = 488 nm). Live A549 cells were incubated with the complex (1 μM) in duplicate for 2 h. After incubation, while one set was irradiated in red light (λ = 600-720 nm; light dose = 30 Joules cm^{-2}) after adding DCFDA, the other one was left unexposed. The strong green fluorescence observed in the photo-irradiated cells implicated ROS generation by **2** in the cellular environment. The complex thus can behave as a therapeutic agent with a dual mode in which singlet oxygen as the ROS in desirable PDT mode involving complex **2** and an active cisplatin species generated on red light activation in a minor chemotherapeutic mode. In contrast, the unexposed cells gave only negligible green fluorescence. A control set was also included with DCFDA stained cells without any treatment, which did not display any changes in fluorescence upon photoexcitation.

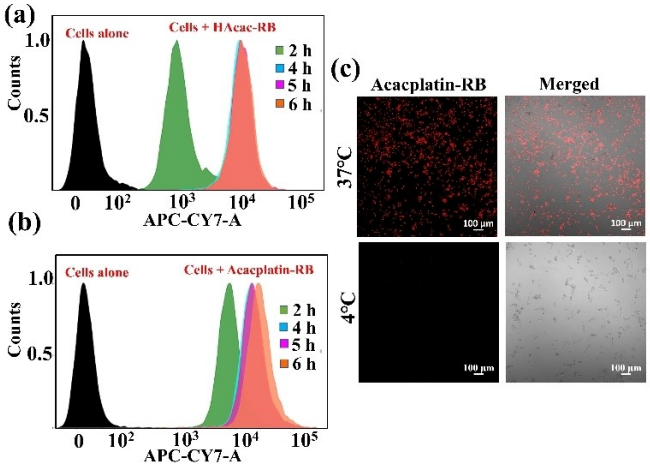

Figure 5. Time dependent analysis of cellular internalisation of the compounds by flow cytometry upon incubating A549 cells with the ligand **HAcac-RB** (1 μM) (a) and its complex **Acacplatin-RB** (1 μM) (b). (c) Confocal images of A549 cells incubated for 4 h with complex **Acacplatin-RB** (1 μM) at two different temperatures, namely, 37 °C and 4 °C.

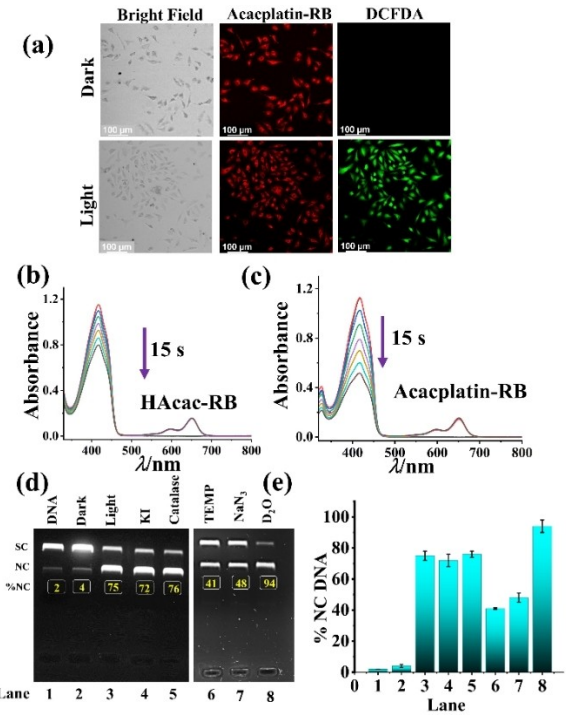

Figure 6. (a) Intracellular ROS detection by DCFDA assay using confocal microscopy. Fluorescence microscopic images of unexposed and light-irradiated (λ = 600-720 nm; light dose = 30 Joules cm^{-2}) A549 cells treated with **Acacplatin-RB** (**2**) [scale bar = 100 μm]. (b, c) A decrease in the absorption maxima of DPBF on red-light irradiation (λ = 642 nm) in the presence of ligand **HAcac-RB** (b) and **Acacplatin-RB** (c) in DMSO solution. This experiment was performed in triplicates. (d) Mechanistic analysis of pUC19 DNA by complex **2** upon 642 nm (100 mW) diode laser exposure for 15 min. pUC19 DNA was incubated with the complex and other additives for 1 h, followed by irradiation with light for 15 min: lane 1, DNA control; lane 2, DNA + **2** in dark; lane 3, DNA + **2** in light; lane 4, DNA + **2** + KI; lane 5, DNA + **2** + Catalase; lane 6, DNA + **2** + TEMP; lane 7, DNA + **2** + NaN_3; lane 8, DNA + **2** in D_2O. (e) A bar diagram representation of two panels shown in (d) with lanes 1–5 and lanes 6–8.

One of the objectives of using a suitably designed BODIPY dye as a photosensitizer is for its efficient photo-generation of singlet oxygen property. ROS has very short lifetime and a small diffusion coefficient with a small radius of action (~100 nm).[33] Besides, there is no apparent naturally occurring defence mechanism against singlet oxygen. To evaluate any formation of singlet oxygen, 1,3-diphenylisobenzofuran (DPBF) experiment was done using this trapping agent of $^1O_2$. In this method, the absorption maximum of DPBF diminishes in the presence of singlet oxygen (Figure 6(b),(c)). The experiment was performed at low concentrations of the dyes (optical density ~0.15) to avoid any self-quenching. The reduction in absorbance of DPBF (at $\lambda = 417$ nm) in the presence of complex **2** or ligand **HAcac-RB** was studied by using a 642 monochromatic red light diode laser and methylene blue ($\Phi_\Delta = 0.52$) as standard. The decrease of absorbance was much faster in the case of complex **2** as compared to **HAcac-RB**. The singlet oxygen quantum yield values measured for the complex and the ligand are 0.36 and 0.18, respectively. The Φ_Δ data support the superior PDT effect of complex **2** when compared to its free BODIPY ligand based on their efficacy of singlet oxygen generation.

The true nature of the ROS formed from complex **2** was unequivocally established from the photoactivated DNA cleavage experiments using different radical scavengers and singlet oxygen quenchers. Supercoiled (SC) pUC19 DNA was used as a convenient biomolecule to monitor its conversion to other forms in presence of the photo-generated ROS. The closed loop SC DNA (native structure, form I) on cleavage forms nicked circular (NC, single strand break, form II) or double nicked, linear (double strand break, form III).[34] Gel electrophoresis was used to determine the rate of migration of different forms of that follows decreasing order from form-I (SC) > form-III (linear) > form-II (NC). The pUC19 DNA (30 μM, 2686 base pairs) was incubated with 10 μM of **Acacplatin-RB** (**2**) for 1 h in 10% DMF-Tris HCl buffer solution at 37 °C. Electrophoretic patterns of cleaved DNA are presented in Figure 6(d). Upon red light irradiation (diode laser $\lambda = 642$ nm for 15 min) of pUC19 DNA with **2**, ethidium bromide (EB) containing agarose gel displayed ~75% of NC DNA and only ~4% in the dark control, indicating photo-cleavage activity of the complex. This also ruled out any dark toxicity arising from this complex. To ascertain the nature of ROS generated by it on red light irradiation, similar experiments were carried out in the presence of different ROS quenchers/scavengers. A significant drop to ~41% and ~48% cleavage was detected in the presence of TEMP (2,2,6,6-tetramethyl-4-piperidone) and sodium azide, both as singlet oxygen quenchers. An increase in photocleaving activity was observed in D_2O in which the lifetime of singlet oxygen is higher than in aqueous buffer. Adding KI (hydroxyl radical scavenger) and catalase (peroxide scavenger) had no inhibitory effect on the DNA scission. This ruled out the formation of any hydroxyl radical or H_2O_2 as ROS. The results unequivocally indicated the formation of singlet oxygen ($^1O_2$) as the sole ROS. This observation is important as formation of singlet oxygen as ROS via type-II photo-process is an essential requirement in PDT.

Subcellular Localization

The red emission of **Acacplatin-RB** (**2**) allowed its use for cellular imaging experiments, and therefore, its intracellular distribution can be analysed. A549 cells treated with **2** (1 μM) were incubated for 3 h at 37 °C, and its distribution to different organelles was examined using confocal laser scanning microscope. Different organelles were individually stained using commercially available dyes. Complex **2** displayed preferential co-localization in mitochondria with a significant overlap with MTG (Mito Tracker Green) giving Pearson's Correlation Coefficient (PCC) value of 0.65. The panels shown in Figure 7 did not display any overlap of complex **2** with the blue emission of nuclear staining Hoechst dye. In addition, moderate co-localization with Endoplasmic Reticulum (ER) was observed giving a PCC value of only 0.43 (Figure S21). Thus, the complex primarily localizes to the mitochondria (mt) and can possibly induce apoptosis through mitochondrial pathways such as caspase activation or mt-DNA interaction with active cisplatin species.[35]

Mitochondrial membrane potential

Photoinduced oxidative stress generated by the BODIPY complex **2** and its prominent localization in the mitochondria of A549 cells led us to examine changes in mitochondrial integrity. The decrease of the mitochondrial membrane potential ($\triangle\Psi_m$) is an important cellular event in the early phase of mitochondrial damage. Modifications in the $\triangle\Psi_m$ were assessed using dual emissive 5,5,6,6′-tetrachloro-1,1′,3,3′-tetraethylbenzimidazoyl carbocyanine iodide (JC-1) dye as the detection probe. In healthy functioning cells, mitochondria have high membrane potential. JC-1, being a cationic lipophilic dye, clumps together in a negatively charged mitochondrial matrix to produce red fluorescence. In contrast, when mitochondria are impaired, their membrane potential drops and JC-1 remains in monomeric form emitting green fluorescence in the cytoplasm.[36] Carbonyl cyanide-p-trifluoromethoxyphenylhydrazone (FCCP), was used as a positive control as it induces strong acidification in mitochondria and completely depolarise $\triangle\Psi_m$. The complex (1 μM) was initially treated with A549 cells in duplicate sets for 4 h, post-removal of the treated compound, one of them was photo-exposed ($\lambda = 600$–720 nm; light dose = 30 Joules cm^{-2}),

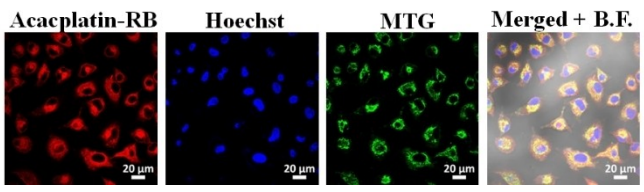

Figure 7. Confocal microscopic images of the complex **Acacplatin-RB** (1 μM) (excitation/emission: 630/670 nm) showing red emission in A549 cells on 3 h incubation in the dark (first image from left). Second and third images display Hoechst (excitation/emission: 352/454 nm) as the nuclear staining dye and Mito tracker green, MTG (excitation/emission: 490/516 nm) as mitochondria staining dye. The merged one as fourth image shows significant mitochondrial localization of **Acacplatin-RB** (**2**). The scale bar is 20 μm. B. F. is Bright Field.

while the complementary set was kept in dark. Strong red and weak fluorescent green signals were duly observed in the unexposed set of cells (Figure 8). The photo-irradiation diminished red emission intensity with a concomitant increase in the green signal. Thus, the complex-mediated disruption of mitochondrial membrane potential was duly observed selectively on red light irradiation and this change initiates various pro-apoptotic factors.

Wound Healing Assay

Migration is one of the significant aspects in the multistep process of carcinogenesis and constitutes an important target for cancer chemoprevention. To examine if our molecule could also affect this process, a wound-healing assay was performed in the presence of **Acacplatin-RB** (**2**), on the metastatic properties of a confluent monolayer of lung carcinoma cells. As depicted in Figure 9, following the initial "wound" on the cell monolayer, clear and well-defined wound borders were observed in both control and treated cell monolayers. The cells were imaged every hour till 12 h. Over time, the borders of the wound gradually closed, by the movement of cells from surrounding areas. This process continued until the wound area eventually disappeared completely within 12 h of incubation. Meanwhile, cell migration at the wound's border in the **Acacplatin-RB** (50 μM) treated cells, was reduced significantly and the healing was not complete even after 12 h of incubation. This suppressed healing clearly indicates that **Acacplatin-RB** exhibits anti-metastatic effects on lung carcinoma cells and may play a crucial role in suppressing the pathways responsible for cancer cell migration.

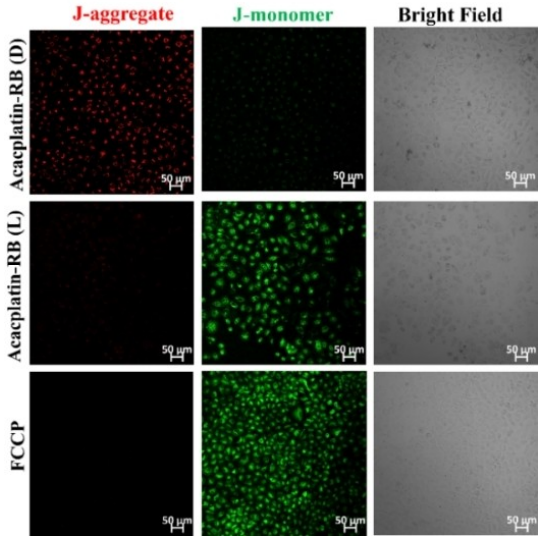

Figure 8. Confocal microscopic images of A549 cells treated with **Acacplatin-RB** (1 μM) and stained with JC-1 dye (excitation: 514 nm; emission: 529 and 590 nm) to detect changes in mitochondrial membrane potential. Experiment was performed in two sets; one set was kept in dark (D) and the other was photo-irradiated (L) using a photoreactor (λ = 600-720 nm; light dose = 30 Joules cm^{-2}) after 4 h incubation at 37 °C. The experiment was performed in triplicates. The scale bar is 50 μm.

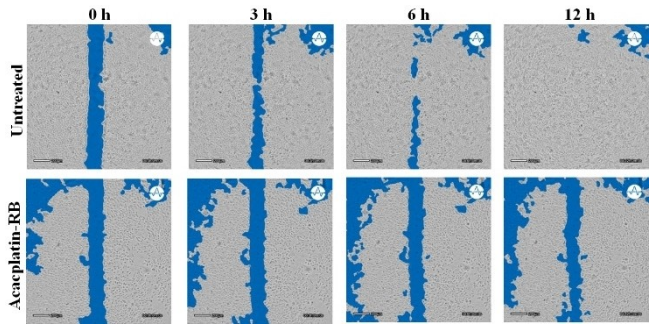

Figure 9. Representative scratch assay images of A549 cancer cells and the effect of treating with **Acacplatin-RB** (50 μM) on wound closure; images at 0, 3, 6, and 12 h following insertion of a scratch/wound. The monolayer was imaged using CytoSMART Lux 2.

Immunostaining of β-tubulin

The tubulin-microtubular system plays a crucial role in the cytoskeleton structures. It is widely recognized that mitochondria exhibit significant interactions with tubulin.[37] Therefore, perturbations in the morphology of microtubules of A549 cells, upon photo-irradiation, were studied using Immunofluorescence assay for beta-tubulin (Figure 10(a)). The microtubules of

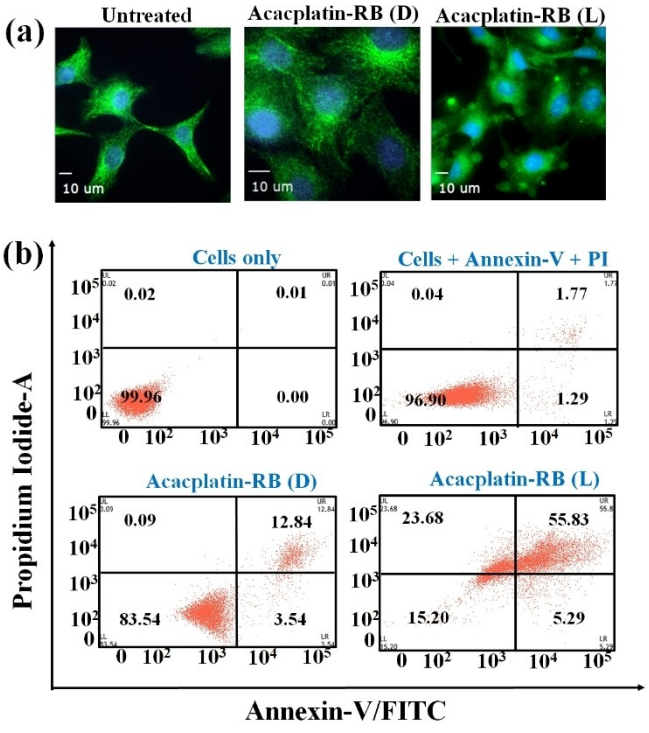

Figure 10. (a) Untreated; **Acacplatin-RB** (**2**, 2 μM) treated A549 cells, kept in dark (D) and upon red light irradiation (L, λ = 600-720 nm; light dose = 30 Joules cm^{-2}) displaying normal and disrupted microtubules. Cells were probed with β-tubulin antibody, followed by Anti rabbit Alexa 488 fluorescent secondary antibody. Scale bar = 10 μm. (b) Scatter plots obtained from the Annexin-V/fluorescein isothiocyanate (FITC) /Propidium Iodide (PI) assay with A549 cells treated with the complex **Acacplatin-RB** (**2**) and exposed to red light (L, λ = 600-720 nm) or incubated in the dark (D) for 4 h. The experiments were performed in triplicates.

unexposed cells revealed a filamentous microtubule network (like that of control) that spans the entire cell, with strong microtubule staining concentrated in a specific perinuclear region associated with the microtubule organisation centre (MTOC). Whereas the filamentous morphology of photo-exposed cells appeared to be disrupted and uniform fluorescence was observed throughout the cell. Also, drastic changes in cellular morphology were observed as cells appeared to be undergoing apoptosis. Thus, significant differences in the characteristic structure of microtubules appeared as a distinguishing feature of cellular damage induced on photo-irradiation.

Cellular Apoptosis

A clear effect was observed on mitochondria and microtubules. It is well established that mitochondria are the integrated centers for intrinsic apoptotic factors.[38] Since complex **Acacplatin-RB** (**2**) successfully perturbs the mitochondrial membrane potential, it boosts the probability of initiating apoptosis via mitochondrial damage. This possibility of apoptosis was examined using Annexin-V/FITC (fluorescein isothiocyanate) and propidium iodide staining of A549 cells treated with the complex. Positive staining of Annexin-V/FITC relies on its selective labelling of early apoptotic cells, and this population can be identified in the lower-right quadrant of dot plots shown in Figure 10(b). Propidium iodide stains the late apoptotic or necrotic cells with disintegrated membranes. Consistent with the previous results, light-irradiated cells displayed a significant apoptotic cell population. The results showed negligible cell death in dark conditions. Complex **2** was thus able to promote cellular apoptosis in a photo-selective manner.

Experimental Section

Materials and Methods

The reagents and chemicals were procured from commercial sources. They were utilized in the received form. Ligand **HAcac-RB** and the complexes **DPP-Pt** and **Acacplatin-RB** were synthesized using modified reported procedures.[26,28] The instruments and methods used for biological characterization and other studies are described as Supporting Information (SI).

Synthetic procedures

Precursor compounds **A-F** were synthesised following methods reported in the literature (Scheme S1, vide supporting information for details).[28] Ligand **HAcac-RB** was synthesised using these precursors and the complexes **DPP-Pt** and **Acacplatin-RB** were synthesised from cisplatin as a starting material. The synthesis and characterization details of **HAcac-RB**, **DPP-Pt** (**1**) and **Acacplatin-RB** (**2**) are given below.

Ligand HAcac-RB

A solution of precursor **F** (387 mg), 4,4-difluoro-8-(4-iodophenyl)-1,7-tetramethyl-3,5-[(4-methoxyphenyl)ethenyl]-4-bora-3a,4a-diaza-s-indacene, in 3 : 1 (v/v) THF/TEA (triethylamine) i.e., 9 : 3 mL was degassed with **B** ((Z)-4-hydroxy-3-(4-iodophenyl)pent-3-en-2-one) (200 mg) using freeze-pump-thaw cycles followed by N_2 purging for 15 min (Scheme S1). $[Pd(PPh_3)_4]$ (35 mg) and CuI (15 mg) were then added and this solution was heated at 60 °C. The solution was stirred for 20 h. Subsequently, the reaction mixture was poured into a saturated solution of ammonium chloride and was extracted using CH_2Cl_2 (3×20 mL). The organic phase was washed with water and brine solution and finally dried over sodium sulphate. Solvents were removed using rotavapor and the purified product was obtained in 0.5% methanol in CH_2Cl_2 using silica gel column chromatography.

Product isolated as a dark blue solid (Yield = 65%, 326 mg). $C_{48}H_{41}BF_2N_2O_4$ (M.W. = 758.6728): C, 75.99; H, 5.45; N, 3.69. Found: C, 75.69; H, 5.67; N, 3.78. ^{1}H NMR (500 MHz, $CDCl_3$) [δ (ppm)]: 7.71 (2H, d, J = 8 Hz), 7.63 (10H, m), 7.38 (2H, d, J = 8 Hz), 7.23 (2H, d, J = 7.4 Hz), 6.96 (4H, d, J = 8.4 Hz), 6.65 (2H, s), 3.88 (6H, s), 1.95 (6H, s), 1.53 (6H, s) (s, singlet; d, doublet; m, multiplet). ^{13}C NMR (125 MHz, $CDCl_3$) [δ (ppm)]: 190.77, 160.49, 137.42, 132.11, 131.91, 130.37, 129.09, 126.04, 123.87, 122.19, 117.71, 114.28, 90.22, 89.39, 55.39, 24.16, 14.85. ESI-MS in acetonitrile (m/z): calcd $[M+Na]^+$, 781.3060; found $[M+Na]^+$, 781.3011. UV-visible in 1 : 1 (v/v) DMSO/DPBS buffer [λ_{max}/nm (ε/M^{-1} cm^{-1})]: 377 (5.6×10^4), 601 (3.1×10^4), 651 (8.8×10^4). Emission spectrum in 1 : 1 (v/v) DMSO/DPBS buffer λ_{em} (λ_{ex}, Φ_F) = 670 nm (630 nm, 0.19).

Platinum(II) complexes 1 and 2

Cisplatin (100 mg, 0.334 mmol) was dissolved in 5 mL of dimethylformamide along with 1.9 equiv. of $AgNO_3$ (107 mg, 0.633 mmol) and stirred for 24 h. A white precipitate of AgCl thus obtained was filtered and removed. The filtrate was added to a deprotonated solution of 1,3-diphenyl-1,3-propanedione (75 mg, 0.334 mmol) for **DPP-Pt** (**1**) or **HAcac-RB** (260 mg, 0.334 mmol) for **Acacplatin-RB** (**2**) in DMF (20 mL) under N_2 atmosphere. An excess of triethylamine (209 μL, 0.501 mmol) was added to deprotonate the ligands. This mixture was stirred for 8 h at room temperature. The solution was then subjected to evaporation in vacuum to obtain a concentrated solution. Subsequent addition of diethyl ether led to the formation of the precipitate of the respective complex, which was separated and washed thoroughly with cold ethanol and diethyl ether to remove any unreacted reactants.

DPP-Pt (1)

Isolated as yellow crystalline solid (Yield = 78%, 134 mg). $C_{15}H_{17}N_3O_5Pt$ (M.W. = 514.4010): C, 35.02; H, 3.33; N, 8.17. Found: C, 35.19; H, 3.56; N, 8.35. ^{1}H NMR (500 MHz, DMSO-D_6): [δ (ppm)], 8.20 (4H, d, J = 8 Hz), 7.66 (2H, t, J = 7 Hz), 7.50 (4H, t, J = 7 Hz), 7.05 (1H, s), 4.84 (6H, s) (t, triplet). ^{13}C NMR (125 MHz, MeOD): [δ (ppm)], 178.43, 136.99, 131.37, 128.45, 126.88, 95.93. ESI-MS in acetonitrile (m/z): calcd $[M–NO_3]^+$, 452.0889; found $[M–NO_3]^+$, 452.0997. UV–visible in 1 : 1 (v/v) DMSO/DPBS buffer [λ_{max}/nm (ε/M^{-1} cm^{-1})]: 331 (3.1×10^4), 383 (1.6×10^4). Λ_M ($S\,m^2\,M^{-1}$) in DMSO: 68.

Acacplatin-RB (2)

Isolated as dark blue solid (Yield = 62%, 204 mg). $C_{48}H_{46}BF2\ N_5O_7Pt$ (M.W. = 1048.8148): C, 54.97; H, 4.42; N, 6.68. Found: C, 55.25; H, 4.70; N, 6.95. ^{1}H NMR (500 MHz, DMSO-D_6) [δ (ppm)]: 7.84 (2H, m), 7.59 (10H, m), 7.41 (4H, d, J = 16 Hz), 7.05 (4H, d, J = 8 Hz), 6.98 (2H,

s), 4.59 (6H, s, broad), 3.83 (6H, s), 1.46 (12H, s). ESI-MS in acetonitrile (m/z): calcd $[M–NO_3]^+$, 986.3215; found $[M–NO_3]^+$, 986.3242. UV – visible in 1:1 (v/v) DMSO/DPBS buffer [λ_{max}/nm (ε/$M^{-1}\,cm^{-1}$)]: 377 (5.6×10^4), 601 (3.1×10^4), 652 (7.3×10^4). Emission spectrum in 1:1 (v/v) DMSO/DPBS buffer λ_{em} (λ_{ex}, Φ_F) = 673 nm (630 nm, 0.07). Λ_M ($S\,m^2\,M^{-1}$) in DMSO: 74.

Conclusions

The red-light active ligand **HAcac-RB** having acetylacetone appended to distyryl-BODIPY unit and its platinum(II) complex $[Pt(NH_3)_2$(**Acac-RB**)$]NO_3$ (**2**, named as **Acacplatin-RB**) were designed and developed as red-light PDT agents showing remarkable photocytotoxicity within the therapeutic spectral window. Complex $[Pt(NH_3)_2(pacac)]NO_3$ (**1**), named as **DPP-Pt**, is prepared and studied as a control species. The BODIPY–Pt(II) complex **Acacplatin-RB** displayed significantly higher photocytotoxicity than the ligand **HAcac-RB** in A549 and MDA-MB-231 cells, giving IC_{50} values in the range of 0.9-1.8 μM. Thls exemplifies the important role of platinum (Pt) in the metal-based PDT chemistry. **DPP-Pt** which lacks a photosensitizer remained essentially inactive in both dark and light. **Acacplatin-RB** (**2**) showed rapid cellular uptake into A549 cancer cells through energy-dependent pathway. As evident from the DCFDA assay, this complex photogenerated ROS in a facile manner in cellular environment. It showed sole formation of highly cytotoxic singlet oxygen ($^1O_2$) thus satisfying one of the prime requirements of PDT besides the use of red-light for photoactivation. Further, excellent molar absorptivity coefficient (ε) value and emissive features in the biological window enable their use in cellular tracking and make them potential theragnostic agents. Complex **2** showed prominent subcellular accumulation in mitochondria and induced loss of mitochondrial membrane potential as observed through JC-1 assay. Interestingly, this chemo-adjuvant demonstrated effective anti-metastasis effect on lung carcinoma cells *in vitro*. Further, complex **2** disrupted the microtubule assembly in a photo-selective manner and induced a desirable apoptotic mode of cell death on photo-irradiation as observed from Annexin V-FITC/propidium iodide assay. This work exemplifies how an organic BODIPY dye, which is a relatively less active PDT agent, can be transformed into a highly efficient photosensitizer on metalation to platinum(II) showing a remarkable overall improvement in the singlet oxygen quantum yield (SOQY) resulting from a facile intersystem crossing (ISC) via a type-II energy transfer pathway.

Supporting Information

The authors have cited additional references and presented results pertaining to this work as the Supporting Information (SI).[S1-S10]

Acknowledgements

A.R.C. thanks the Department of Science and Technology (DST SERB), Government of India, for financial support (CRG/2018/000081) and for J. C. Bose national fellowship (SR/S2/JCB-26/2007). A. R. C. thanks the Indian National Science Academy (INSA), New Delhi, for Senior Scientist fellowship (INSA/SP/SS/2021). D.K.S.'s research group is funded by grant from SERB (CRG/2020/000239). We are thankful to Urvashi for FACS data and to Suchetha for confocal microscopy images.

Conflict of Interests

There are no conflicts to declare.

Data Availability Statement

The data that support the findings of this study are available from the corresponding author upon reasonable request.

Keywords: Bioinorganic chemistry · Platinum · Boron-dipyrromethene · Photodynamic therapy · Singlet oxygen

[1] K. Wang, C. Zhu, Y. He, Z. Zhang, W. Zhou, N. Muhammad, Y. Guo, X. Wang, Z. Guo, *Angew. Chem. Int. Ed.* **2019**, *131*, 4686–4691.
[2] a) D. Hu, C. Yang, C. N. Lok, F. Xing, P. Y. Lee, Y. M. E. Fung, H. Jiang, C. M. Che, *Angew. Chem. Int. Ed.* **2019**, *58*, 10914–10918; b) F. M. Muggia, A. Bonetti, J. D. Hoeschele, M. Rozencweig, S. B. Howell, *J. Clin. Oncol.* **2015**, *33*, 4219–4226; c) A. Casini, J. Reedijk, *Chem. Sci.* **2012**, *3*, 3135–3144.
[3] C. A. Wootton, C. Sanchez-Cano, A. F. Lopez-Clavijo, E. Shaili, M. P. Barrow, P. J. Sadler, P. B. O'Connor, *Chem. Sci.* **2018**, *9*, 2733–2739.
[4] a) R. C. Todd, S. J. Lippard, *Metallomics* **2009**, *1*, 280–291; b) T. C. Johnstone, K. Suntharalingam, S. J. Lippard, *Chem. Rev.* **2016**, *116*, 3436–3486; c) R. G. Kenny, C. J. Marmion, *Chem. Rev.* **2019**, *119*, 1058–1137.
[5] J. Mlcouskova, J. Stepankova, V. Brabec, *J. Biol. Inorg. Chem.* **2012**, *17*, 891–898.
[6] P. Štarha, Z. Trávníček, Z. Dvořák, T. Radošová-Muchová, J. Prachařová, J. Vančo, J. Kašpárková, *PLoS One* **2015**, *10*, e0123595.
[7] K. Mitra, S. Gautam, P. Kondaiah, A. R. Chakravarty, *Angew. Chem. Int. Ed.* **2015**, *127*, 14195–14199.
[8] K. Mitra, S. Gautam, P. Kondaiah, A. R. Chakravarty, *Eur. J. Inorg. Chem.* **2017**, *12*, 1753–1763.
[9] V. Ramu, S. Gautam, A. Garai, P. Kondaiah, A. R. Chakravarty, *Inorg. Chem.* **2018**, *57*, 1717–1726.
[10] K. Mitra, C. E. Lyons and M. C. T. Hartman, *Angew. Chem. Int. Ed. Int. Ed.* **2018**, *130*, 10420–10424.
[11] A. P. Castano, T. N. Demidova, M. R. Hamblin, *Photodiagn. Photodyn. Ther.* **2005**, *2*, 1–23.
[12] J. Schuitmaker, H. van Leengoed, F. van der Meulen, W. Star, N. van Zandwijk, *J. Photochem. Photobiol. B* **1996**, *34*, 3–12.
[13] a) C. A. Robertson, D. H. Evans, H. Abrahamse, *J. Photochem. Photobiol. B* **2009**, *96*, 1–8; b) K. Han, S. B. Wang, Q. Lei, J. Y. Zhu, X. Z. Zhang, *ACS Nano* **2015**, *9*, 10268–10277.
[14] S. Kolemen, M. Işık, G. M. Kim, D. Kim, H. Geng, M. Buyuktemiz, T. Karatas, X. F. Zhang, Y. Dede, J. Yoon, E. U. Akkaya, *Angew. Chem. Int. Ed.* **2015**, *127*, 5430–5434.
[15] a) M. D. Yaqoob, L. Xu, C. Li, M. M. L. Leong, D. D. Xu, *Photodiagn. Photodyn. Ther.* **2022**, *38*, 102830; b) W. Fan, P. Huang, X. Chen, *Chem. Soc. Rev.* **2016**, *45*, 6488–6519.
[16] A. Bera, S. Gautam, S. Sahoo, A. K. Pal, P. Kondaiah, A. R. Chakravarty, *RSC Med. Chem.* **2022**, *13*, 1526–1539.
[17] M. Ochsner, *J. Photochem. Photobiol. B.* **1996**, *32*, 3–9.
[18] A. Loudet, K. Burgess, *Chem. Rev.* **2007**, *107*, 4891–4932.

[19] Y. Ni, J. Wu, *Org. Biomol. Chem.* **2014**, *12*, 3774–3791.
[20] A. Kamkaew, S. H. Lim, H. B. Lee, L. V. Kiew, L. Y. Chung, K. Burgess, *Chem. Soc. Rev.* **2013**, *42*, 77–88.
[21] a) A. Turksoy, D. Yildiz, E. U. Akkaya, *Coord. Chem. Rev.* **2019**, *379*, 47–64; b) Y. Wu, S. Li, Y. Chen, W. He, Z. Guo, *Chem. Sci.* **2022**, *13*, 5085–5106.
[22] a) C. S. Kue, S. Y. Ng, S. H. Voon, A. Kamkaew, L. Y. Chung, L. V. Kiew, H. B. Lee, *Photochem. Photobiol. Sci.* **2018**, *17*, 1691–1708; b) L. Wang, Y. Qian, *Biomater. Sci.* **2023**, *11*, 1459–1469.
[23] X. F. Zhang, X. Yang, *J. Phys. Chem. B* **2013**, *117*, 9050–9055.
[24] K. Chen, Y. Dong, X. Zhao, M. Imran, G. Tang, J. Zhao and Q. Liu, *Front. Chem.* **2019**, *7*, 821.
[25] X. J. Jiang, J. T. F. Lau, Q. Wang, D. K. P. Ng, P. C. Lo, *Chem. Eur. J.* **2016**, *22*, 8273–8281.
[26] A. Upadhyay, P. Kundu, V. Ramu, P. Kondaiah, A. R. Chakravarty, *Inorg. Chem.* **2022**, *61*, 1335–1348.
[27] V. Ramu, P. Kundu, P. Kondaiah, A. R. Chakravarty, *Inorg. Chem.* **2021**, *60*, 6410–6420.
[28] J. H. Olivier, A. Haefele, P. Retailleau, R. Ziessel, *Org. Lett.* **2010**, *12*, 408–411.
[29] a) L. S. Kassel, *J. Chem. Phys.* **1936**, *4*, 276–282; b) A. D. Becke, *J. Chem. Phys.* **1993**, *98*, 5648–5652 (vide SI for details).
[30] a) J.-B. Lepecq, C. Paoletti, *J. Mol. Biol.* **1967**, *27*, 87–106; b) R. L. Jones, A. C. Lanier, R. A. Keel, W. D. Wilson, *Nucleic Acids Res.* **1980**, *8*, 1613–1624; c) J. Yao, P. T. Lowary, J. Widom, *Proc. Natl. Acad. Sci. USA* **1993**, *90*, 9364–9368.
[31] a) X. Xue, C. Qian, H. Fang, H. Liu, H. Yuan, Z. Guo, Y. Bai, W. He, *Angew. Chem. Int. Ed. Int. Ed.* **2019**, *131*, 12791–12796; b) A. Bera, S. Gautam, M. K. Raza, A. K. Pal, P. Kondaiah, A. R. Chakravarty, *Dalton Trans.* **2022**, *51*, 3925–3936.
[32] a) V. Ramu, P. Kundu, A. Upadhyay, P. Kondaiah, A. R. Chakravarty, *Eur. J. Inorg. Chem.* **2021**, *2021*, 831–839; b) V. Ramu, S. Gautam, P. Kondaiah, A. R. Chakravarty, *Inorg. Chem.* **2019**, *58*, 9067–9075; c) M. K. Raza, S. Gautam, A. Garai, K. Mitra, P. Kondaiah, A. R. Chakravarty, *Inorg. Chem.* **2017**, *56*, 11019–11029; d) M. K. Raza, S. Gautam, P. Howlader, A. Bhattacharyya, P. Kondaiah, A. R. Chakravarty, *Inorg. Chem.* **2018**, *57*, 14374–14385.
[33] M. Li, J. Xia, R. Tian, J. Wang, J. Fan, J. Du, S. Long, X. Song, J. W. Foley, X. Peng, *J. Am. Chem. Soc.* **2018**, *140*, 14851–14859.
[34] R. Palchaudhuri, P. J. Hergenrother, *Curr. Opin. Biotechnol.* **2007**, *18*, 497–503.
[35] J. Morgan, A. R. Oseroff, *Adv. Drug Delivery Rev.* **2001**, *49*, 71–86.
[36] F. Sivandzade, A. Bhalerao, L. Cucullo, *Bio. Protoc.* **2019**, *9*, e3128.
[37] L. C. Woods, G. W. Berbusse, K. Naylor, *Front. Cell. Dev. Biol.* **2016**, *4*, 19.
[38] D. C. Wallace, *Nat. Rev. Cancer* **2012**, *12*, 685–698.

Manuscript received: July 31, 2023
Revised manuscript received: September 11, 2023
Accepted manuscript online: September 14, 2023
Version of record online: September 27, 2023